NONEQUILIRIUM MOLECULAR DYNAMICS METHODS FOR LATTICE HEAT CONDUCTION CALCULATIONS

Junichiro Shiomi

Department of Mechanical Engineering, The University of Tokyo, 7-3-1 Hongo, Bunkyo-ku, Tokyo, 113-8656
Japan Science and Technology Agency, PRESTO, 4-1-8 Hongo, Kawaguchi, Saitama, 332-0012, Japan

Over the last decades, molecular dynamics simulations have been extensively used to calculate lattice heat conduction in nano- and bulk-materials, as the realistic potential functions, software package, and many core clusters have become widely accessible. Nonequilibrium molecular dynamics, particularly the inhomogeneous ones, have been a popular choice of method owing to their intuitive way of applying the perturbation to the system. On the other hand, despite its simplicity, the results can be significantly influenced by the simulation parameters, and various methodological issues such as validity of linear response theory, effect of sizes, influence of temperature or heat flux control need to be carefully checked and taken into account. These aspects are discussed for various types of nonequilibrium methods based on homogeneous/inhomogeneous and steady/transient molecular dynamics simulations. Their capability to calculate bulk thermal conductivity, heat wave propagation, the classical size effect of thermal conductivity at the nanoscale, and total and spectral thermal boundary conductance are explained and demonstrated with examples.

NOMENCLATURE

Acronyms

CNT	carbon nanotube
EMD	equilibrium molecular dynamics
DFT	density functional theory
GK	Green-Kubo
GROMACS	Groningen machine for chemical simulations
HNEMD	homogeneous nonequilibrium molecular dynamics
IFC	interatomic force constant
LAMMPS	large-scale atomic/molecular massively parallel simulator
MD	molecular dynamics
NEMD	nonequilibrium molecular dynamics
NAMD	not another molecular dynamics program
PE	polyethylene
TBR	thermal boundary resistance

Symbols

B	phase variable
C	phase variable
c	phonon specific heat [JK^{-1}]
D	phase variable
F	Hellmann Feynman force [N]
F_e	external force [N]
f	phonon frequency [Hz]
G	Thermal boundary resistance [m^2KW^{-1}]
g	phonon energy spectrum
H_0	Hamiltonian
k	phonon wavevector [m^{-1}]
L	system length [m]
L_c	thermostat length [m]
p	atom momentum [$kgms^{-1}$]
q	heat flux [Wm^{-2}]
r	atom position [m]
S	interface area [m^2]
s	phonon polarization

T	temperature [K]
T_{sp}	spectral temperature [K]
ΔT	temperature difference [K]
ΔT_j	temperature jump [K]
t	time [s]
v	phonon group velocity [ms^{-1}]
$\bar{v}$	average phonon group velocity [ms^{-1}]

Greek Symbols

α	Cartesian component
κ	thermal conductivity [$Wm^{-1}K^{-1}$]
κ_∞	bulk thermal conductivity
Λ	phonon mean free path [m]
τ	phonon mean free path [s]
$\bar{\tau}$	average phonon mean free path [s]
τ_{TH}	thermostat relaxation time [s]
τ_T	temperature relaxation time [s]
ω	phonon angular frequency [Hz]
ω^{max}	maximum phonon frequency [Hz]
ω^{min}	minimum phonon frequency [Hz]
Φ	harmonic interatomic force constant [Nm^{-1}]
Ψ	cubic interatomic force constant [Nm^{-1}]
X	quartic interatomic force constant [Nm^{-1}]

1. INTRODUCTION

Over the last decades, molecular dynamics simulations have become a popular tool to calculate lattice thermal transport properties. It is partly due to the increasing capability of molecular dynamics (MD) simulations, where more complex potential functions have become available, no longer limited to the simple pair potentials such as Lennard-Jones [1] and Morse types [2]. The increasing capability to handle many body interactions has dramatically increased the usability of MD simulations for complex molecules, solids, and interfaces [3, 4]. Furthermore, the first principles calculations have become widely accessible, which gave rise to development of various non-empirical potentials, for instance, the ones tuned for phonon transport properties [5-7]. Together with the growing speed and capacity of computers, one can perform simulations of realistic finite-size materials with non-periodic computational domains. This allows us to carry out heat conduction calculation in intuitive setup, for instance, calculating thermal conductivity directly from the expression of Fourier's law by imposing steady temperature gradient and heat flux to the system.

The capability to calculate thermal transport properties of non-periodic system finds its attraction in relation with nanotechnology. With the development of technology to synthesize and characterize materials at the nanoscale, there has been a great demand to understand and control thermal transport of nanostructures and interfaces [8]. At the nanoscale, thermal transport needs to be thought differently from that at the macroscale, namely in terms of the size effect of the intrinsic heat conduction and the importance of interfaces. At the length scale smaller than the phonon mean free path, thermal energy gradient divided by the heat flux is no longer a unique material property and depends on the size of the system. At the same time, the importance of the interfacial thermal resistance becomes more important with respect to the intrinsic thermal resistance. The nonequilirbium molecular dynamics (NEMD) simulations offer straightforward means to calculate these properties.

The use of NEMD method is not limited to the nanoscale systems. It can be an alternative choice to the counterpart method, the equilibrium molecular dynamics (EMD) simulations, widely used to calculate bulk thermal conductivity through the Green-Kubo (GK) formula based on the linear response theory. The general strategy of NEMD is to calculate thermal conductivity by applying a perturbation to the system and measuring the response. The perturbation can be applied in different ways. Most intuitive and common choice of perturbation would be the steady temperature gradient or heat flux, allowing "direct" extraction of thermal conductivity. Perhaps, more nontrivial way would be to apply the perturbation on the Hamiltonian of the system. In

any case, NEMD methods utilize perturbation to realize faster convergence compared to the GK method. In addition to the steady NEMD methods, there are transient methods that can be useful to separate different time scales imbedded in the system.

The spread of molecular dynamics simulations over the last decade is also attributed to the great progress in their accessibility. There are software packages such as, LAMMPS [9], GROMACS [10], NAMD [11], and DL_POLY [12] that enable even non-experts to easily perform molecular dynamics simulations and calculate variety of properties without having to code almost at all. However, even in the simplest thermal conductivity calculation, such as the direct NEMD methods, there are subtle technical issues that can cause severe error in the calculations [13-16]. To this author's understanding, all the MD methods have their strength and weakness and there is no perfect one. Therefore it is important to understand the capabilities and limits of each method, and to properly apply an appropriate method for each purpose.

The current paper reviews basic methodologies of NEMD methods to characterize lattice heat conduction in solids. Here, NEMD methods are divided into (1) steady inhomogeneous method [17], (2) steady homogeneous method [18], and (3) transient methods [19]. Each method is designed to target different aspects of thermal conductivity and thermal boundary conductance as described in the followings.

2. THERMAL CONDUCTIVITY

2.1 Steady inhomogeneous method

2.1.1 Basic methodology

Since thermal conductivity is a transport coefficient that linearly relates temperature gradient and heat flux, the most intuitive approach would be to apply a steady temperature gradient (heat flux) and measure the heat flux (temperature gradient). When one-dimensional heat conduction is realizable, this can be done simply by sandwiching the system of interest with a heat source and a heat sink. The advantage of the method, in addition to being intuitive, is that it does not require the periodic boundary condition in the direction of heat conduction, and can deal with finite length systems. This can be useful on investigating the size effect of nanoscale materials such as thin films [13, 20, 21] and nanotubes/nanoribbons [22-24]. Such *direct* NEMD can be performed for over hundred nanometers and nanoseconds [14], although it depends on the complexity and interaction length of the potential function. For materials with small cross section such as carbon nanotubes (CNTs), simulations have been performed for over micrometer length [25]. This would require over hundred thousand atoms but the solid thermal conductivity calculation without bond switching can be very efficiently parallelized.

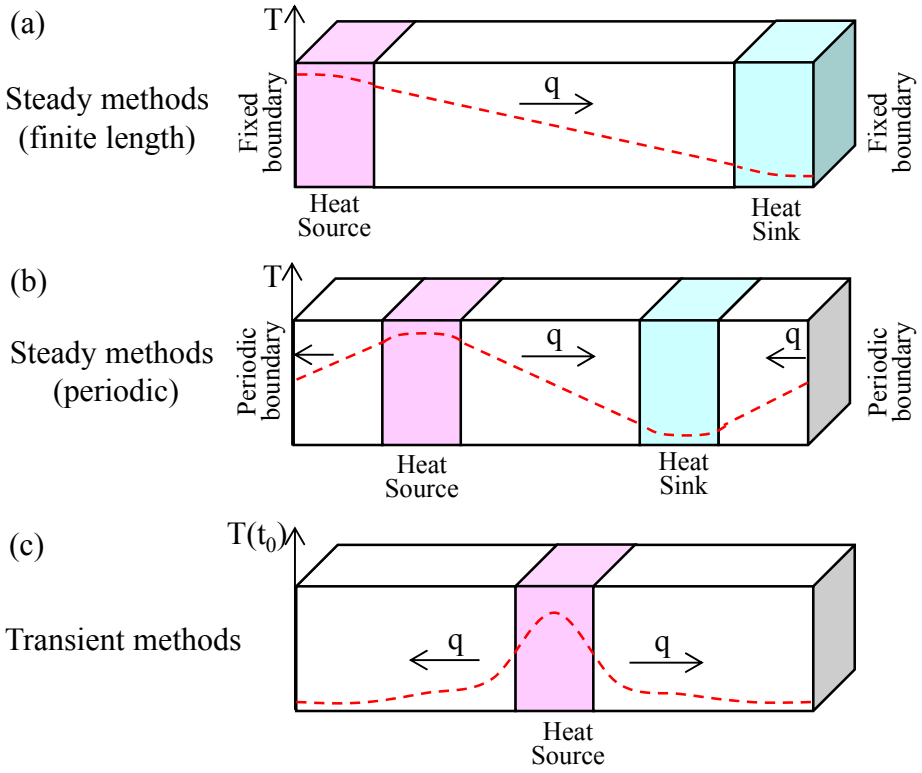

Fig. 1 Schematics of the nonequilibrium molecular dynamics simulations to calculate thermal conductivity. Steady temperature (T) or heat flux (q) methods with (a) finite-length and (b) periodic system, and (c) a transient method.

The direct NEMD methods for thermal conductivity are illustrated in Fig. 1(a, b). A typical simulation begins by equilibrating the entire system at a certain temperature, typically the mean target temperature. Then the temperatures of or energy flux to the ends of the system are controlled to realize the heat source and sink. Eventually, the system converges to a steady state with linear temperature gradient and constant heat flux. The required time to reach convergence generally grows with the system size due to increase in the degrees of freedom. On the other hand, when the system size is comparable to the mean free paths of phonons, increasing the size makes the heat conduction more diffusive, which helps the system to reach the steady sate. Once the steady state is achieved, from the temperature gradient and heat flux, thermal conductivity can be calculated through the Fourier's law,

$$\kappa = -\frac{q}{\partial T/\partial z}, \tag{1}$$

where z is the direction of heat flux.

Despite the simplicity of the simulation, there are several methodological issues that are worth addressing. For instance, for the linear response theory to be applicable, the temperature gradient needs to be sufficiently small. Since it is not possible to prove the applicability *a priori*, it needs to be checked by performing multiple simulations with different temperature gradients and heat fluxes [16]. Yet the linear response theory has been reported to be surprisingly robust, and large temperature gradient (heat flux) in the order of 1 Knm^{-1} (1 μWnm^{-2}) has been shown to give reasonable results [14]. The validity of the local thermodynamic equilibrium on defining the temperature in solids has also been confirmed [13] in a similar manner as in fluids [16, 26], although the validity is certainly questionable for strongly ballistic systems such as short molecular chains.

Another important issue is the choice of boundary conditions. Firstly, one needs to choose whether to control the temperature gradient or heat flux. Then, one can either choose to control temperature using thermostats (e.g. velocity scaling, Nose Hoover [27, 28], Langevin [29]), or to rescale/exchange the velocity vectors in the cold and hot regions [13, 30-33], respectively. Although it has been pointed out that the choice can alter the convergence speed or conservation of momentum and energy, these appear to have little influence to the calculated values of thermal conductivity [13, 15]. However, these are true only when the control methods are properly installed [34], which can be a rather tedious process. This aspect is demonstrated in the following section taking a case of the temperature control approach.

2.1.2 Thermostating

On carrying out the direct NEMD simulations by locally applying the thermostats to a solid, the interface between the temperature-controlled part and the rest of the system often gives rise to a nonlinear temperature profile near the thermostats. This is demonstrated in Fig. 2, taking the case of a CNT [25]. Here, the thermostats at 310 K and 290 K were applied to the ends of a 50-nm-long CNT, and the data were sampled for 18 ns (36 million time steps). The nonlinear profile appears due to mismatching of lattice-vibrational spectra between the temperature controlled part and the rest of the system. The mismatching causes reflection of phonons and alters scattering dynamics at the boundary, and thus, gives rise to local nonequilibrium phonon distribution. When the system length is smaller than the characteristic phonon mean free path, which is the case in the CNT, the nonequilibrium distribution can significantly alter the overall heat conduction. Note that, although the temperature profile around the center appears to be

linear, this only means that at least some of the phonons are transported diffusively, since the ballistic phonons do not contribute to the temperature gradient.

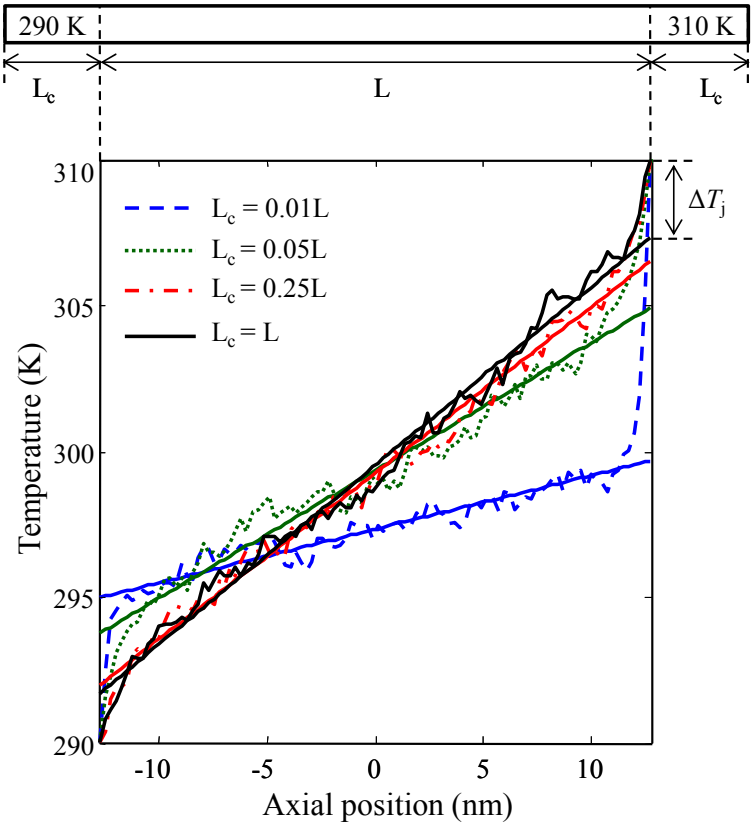

Fig. 2 Influence of the length of the layers controlled by Nose-Hoover thermostat (L_c) on the temperature profile [25]. A case of 25-nm-long (5, 5) carbon nanotube is presented.

One way to quantify the significance of the nonlinear temperature profile or the *temperature jump* ΔT_j at the boundary between thermostated part and the rest is to translate it to thermal resistance $\Delta T_j/q$ (Thermal Boundary Resistance, TBR). Most intuitive approach to calculate thermal conductivity of a finite system is to minimize the TBR by choosing the appropriate thermostat parameters. Here a case with Nose-Hoover thermostat [27, 28] is introduced, although the following discussion can be also applied to other thermostats. The Nose-Hoover thermostats have two tuning parameters; the length of the temperature controlled part L_c and the relaxation time τ_{TH}. Increasing L_c permits larger wavelength phonon modes and hence attenuates the discrepancy of phonon spectra between temperature-controlled part and the rest of the system. This can be seen in the L_c-dependence of the temperature profiles (Fig. 2), where the smaller L_c is,

the larger ΔT_j is. As denoted in the figure, ΔT_j here is obtained by extrapolating the linear temperature profile extrapolated to the boundary and averaged for left and right ends. The influences on the thermal transport (temperature gradient, heat flow, and thermal conductivity) are summarized in Fig. 3(a-c). Both the temperature gradient and heat flux increases with L_c and eventually saturated at the upper limit $L_c \sim L$, where the phonon spectra (more precisely the density of states) of the parts with and without thermostat become identical. In terms of the relaxation time τ_{TH}, TBR exhibits a minimum with a certain τ_{TH} due to the crossover between over and under damping (Fig. 4).

As shown in Fig. 4, the optimal thermostat parameters (τ_{TH} and L_c) also depend on L since the permitted phonon wavelengths change. Therefore, ideally speaking, the parameters need to be tuned for each L when investigating the size effect, which could be rather tedious. Technically speaking, one could include the tuning process into the molecular dynamics iterations, but it appears to be more common in the literature to simply perform a number of different simulations.

It is worth noting that, although the TBR may be thought as a numerical artifact when calculating thermal conductivity of an isolated system, the observed coupling between the TBR and intrinsic heat conduction is an important issue in practical situations, for instance when the system is bounded with connections to other materials. In such case, the heat conduction properties would be inevitably altered by TBRs at the connections. Therefore, in fact, it might be more realistic to examine the heat conduction with presence of TBRs, although formulation of a general case would be difficult since such effects would be strongly case-dependent.

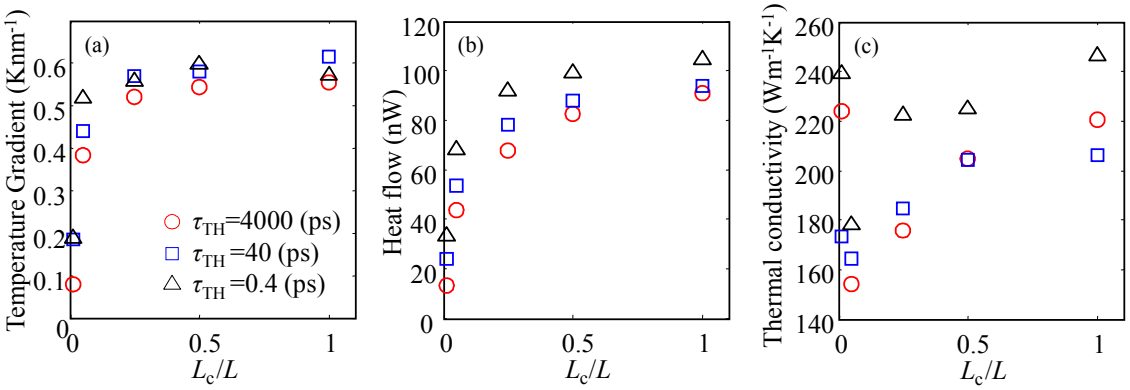

Fig. 3 Influence of thermostat length L_c and relaxation time of Nose-Hoover thermostat τ_{TH} on the temperature gradient, heat flow, and thermal conductivity [25], in a case of 50-nm-long (5, 5) CNT.

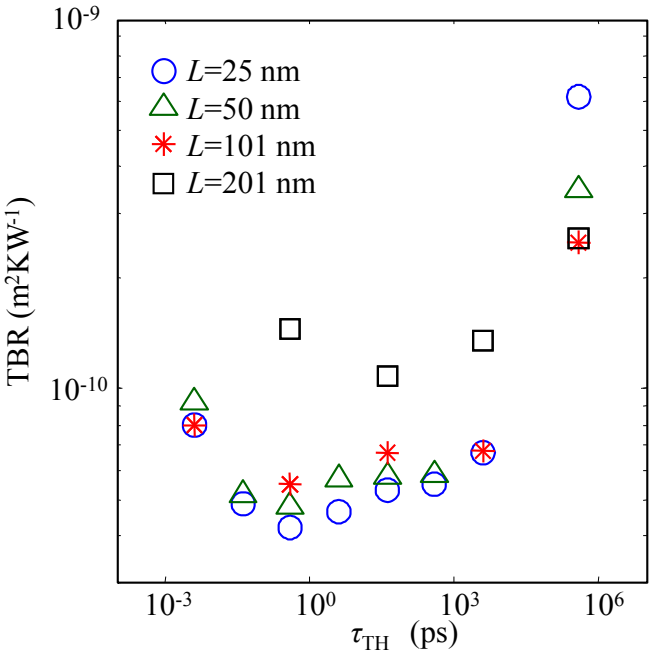

Fig. 4 Influence of the relaxation time of Nose-Hoover thermostat τ_{TH} on TBR [25].

2.1.3 Classical size effect

When the boundary conditions are properly installed, the direct NEMD simulation becomes a powerful tool to calculate the size effect of thermal conductivity. Here we refer this as classical size effect (in contrast to quantum size effect), which arises from the ballistic heat conduction manifesting at small scales [8]. Using the phonon gas kinetics model, this can be described in terms of phonon mean free paths $\Lambda_{k,s}$ and the system length L, where the subscripts k and s are the phonon wavevector and polarization. Let us now base the discussion on the Boltzmann–Peierls description of thermal conductivity [35],

$$\kappa = \frac{1}{3}\sum_{k,s} c_{k,s} v_{k,s} \Lambda_{k,s} , \qquad (2)$$

where $c_{k,s}$ and $v_{k,s}$ are the phonon specific heat and group velocity. Here we stay in the continuum dispersion regime, where $c_{k,s}$ and $v_{k,s}$ are independent of L. We can then divide the heat conduction into three regimes of L: (i) all phonons exhibit $\Lambda_{k,s}$<L (diffusive conduction), (ii) all phonons exhibit $\Lambda_{k,s}$>L (ballistic conduction), and (iii) mixture of (i) $\Lambda_{k,s}$<L and (ii) $\Lambda_{k,s}$>L (quasi-ballistic conduction). The kinetic theory in Eq. (2) gives, for each regime, the length dependence of the thermal conductivity (i) constant, (ii) linear dependence, and (iii) nonlinear dependence. Therefore, as reducing

L starting from the large bulk crystal, thermal conductivity remains constant until L becomes smaller than $\Lambda_{k,s}$ of some of the heat carrying phonons, then decreases nonlinearly until it asymptotically approaches the linear dependence at the small L limit.

Note that this size effect is somewhat different from the one found in periodic systems. As it will be discussed later in details thermal conductivity calculated from a periodic simulation cell can be similarly limited by its finite size due to the missing contribution from the phonons with wave length longer than the cell size. However, due to the periodicity, the phonons are allow to travel longer than the cell size through the periodic boundary and thus the phonon mean free paths are not limit by the cell size. In this sense, the size effect in a periodic system cannot be associated with a real phenomenon, and thus, the periodic simulation is suited for an investigation of the classical size effects.

The usage of thermal conductivity to express the heat conduction with ballistic phonon transport can be argued since thermal conductivity is defined based on the diffusive description (Fourier's law). Therefore simply expressing the heat conduction in terms of thermal conductance should be more suitable at the scale smaller than phonon mean free paths. However, it is often convenient to effectively define the transport coefficient for the sake of continuum representation and comparison with previous studies.

A classical size effect obtained from NEMD is demonstrated here by taking the previous CNT as an example. As shown in Fig. 5, the overall trend of the slope indicates the gradual transition from ballistic to quasi-ballistic heat conduction. The asymptotic match of the data to the dashed line suggests nearly pure ballistic heat conduction at the small L limit. On the other hand, the positive gradient at the upper bound indicates that the limit of the quasi-ballistic heat conduction exceeds a micrometer. Such long quasi-ballistic limit of CNT has been also shown by lattice dynamics [36]. Note that heat is carried not only by the ballistic transport of acoustic phonons but also by that of various optical phonons for a realistic length. Such an active role of optical phonons as heat carriers at the nanoscales has been also discussed for other materials [37], and it is particularly significant for materials with large unit cells such as CNTs.

The length dependence has been compared with a phonon transport model [38], which seamlessly handles the crossover from fully ballistic to diffusive thermal transport regimes,

$$\kappa = \sum_{k,s} c_{k,s} v_{k,s} L \frac{\Lambda_{k,s}}{L + \Lambda_{k,s}} = \frac{1}{2\pi} \sum_{s} \int_{\omega_s^{\min}}^{\omega_s^{\max}} c'(\omega) L \frac{\Lambda'_s(\omega)}{L + \Lambda'_s(\omega)} d\omega , \quad (3)$$

where the prime denotes the frequency-dependent representation. The expression reduces to the Landauer's formula for coherent phonon transport with perfect transmission [39, 40] at the small L limit ($L \to 0$). On the other hand, it reduces to Eq. (2) at the large L limit ($L \to \infty$). The "transmission function" $\Lambda_s'(\omega)/\left[L + \Lambda_s'(\omega)\right]$ can be derived either by describing the phonon-phonon scattering as fictitious probes with the analogy to the electron transport [38] or by applying the Matthiessen's rule at the Casimir limit [41] in mode-dependent fashion. By approximating the mean free paths based on the Klemens' model [42], as seen in Fig. 5, the agreement between NEMD and the phonon transport model is remarkable. This provides a unified picture of the lattice heat conduction in the direct NEMD simulation and the phonon gas kinetics theory.

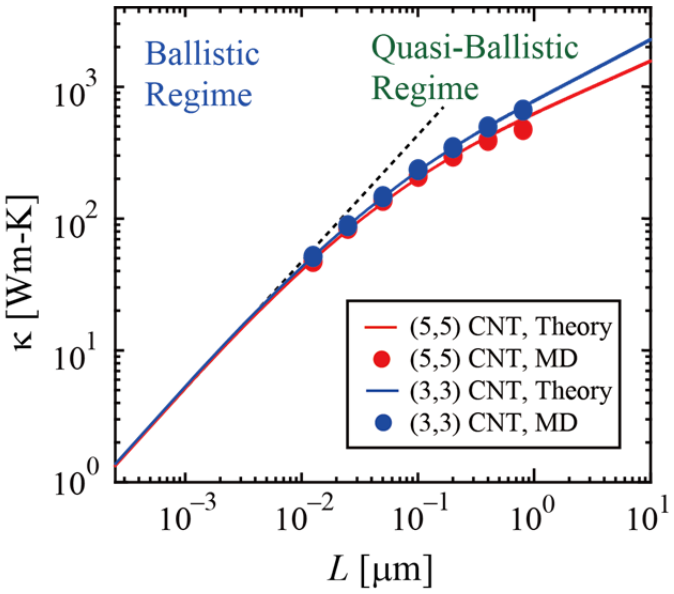

Fig. 5 The classical size effect of carbon nanotube thermal conductivity at room temperature. The blue and red circles are nonequilibrium molecular dynamics data of (3, 3) and (5, 5) carbon nanotubes, respectively. The blue and red solid curves denote the corresponding theoretical model [38].

2.1.4 Bulk thermal conductivity

The direct NEMD methods can be also useful to calculate bulk thermal conductivity with advantage in realizing faster conversion than the GK method. While many of the early works have used simple systems to study the methodological aspects, over the last decade or so, there have been an increasing number of works on more realistic materials

including silica [33, 43], zirconium compounds [44, 45], nanotubes [46], and polymers [47]. NEMD methods also have advantage in calculating systems with complex unitcells, where interpretation of the GK method can be challenging [48]. This aspect has made the NEMD a useful tool to calculate thermal conductivities of superlattice [49-54], nancomposites [55-57], and alloys [58]. For this purpose, simulations with periodic boundary condition can also be useful. As shown in Fig. 1 (b), the simulation of the periodic cell can be realized by imposing two steady-temperature gradients or heat fluxes, which can be done for instance by rescaling or exchanging the velocity vectors in the cold and hot regions [13, 30-33].

Here, we encounter the same problem as the above classical size effect. It has been pointed out by Schelling *et. al.* [14] that phonon scattering at the heat source and sink contributes more than the intrinsic phonon scattering to thermal conductivity unless the simulation cell is many times longer that the phonon mean free paths. Since this may not be affordable in many cases, a common practice is to calculate effective thermal conductivity for various sizes and extrapolate them to the infinite size value. A commonly used function for the extrapolation [59] is

$$\frac{1}{\kappa(L)} = \frac{1}{\kappa_\infty} + \frac{A}{L} \tag{4}$$

where A is a constant. As described by Schelling *et. al.* [14], the expression comes from the Matthiessen's rule at the Casimir limit [41]. The general expression of the mixing rule gives the length dependent relaxation time τ as a function of the relaxation times of intrinsic phonon-phonon scattering τ_∞ and the modeled boundary scattering v/L,

$$\frac{1}{\bar{\tau}(L)} = \frac{1}{\bar{\tau}_\infty} + \frac{\bar{v}}{L}. \tag{5}$$

Here, as denoted with the bar, the properties are averaged over all the phonons, or all the phonons are assumed to have the same properties. Now, assuming $\kappa = c\bar{v}\bar{\Lambda}/3$ to hold, we can derive Eq. (4).

Despite the rather crude approximation with the averaged phonon properties, the scaling has successfully reproduced the values obtained from the GK calculations [14]. The scaling is now widely accepted and has been used by a number of the works [15, 43, 56, 59-67]. On the other hand, since phonon transport properties can be strongly multiscale [68], there should be limits to the range of applicability beyond which the mode dependence matters. Such applicability and limit of the averaged description has been investigated in mode-dependent fashion by Sellan *et. al.* [48], where they find that

thermal conductivity is underestimated when the system size is smaller than the largest mean free paths with dominant contribution to the bulk thermal conductivity.

2.1.5 Interatomic force constants from first principles

In many of the cases reviewed above, the accuracy of the NEMD calculations has been evaluated based on comparison with EMD but not with experiments due to the incompleteness of the potential functions (or force fields). For instance, silicon thermal conductivity obtained by commonly use potentials such as Stillinger Weber [69] and Tersoff [70] have been shown by lattice dynamics calculations to significantly overestimate the experimental values [71]. This has been recently overcome by development of first-principle-based anharmonic interatomic force constants (IFCs). Using lattice dynamics and EMD with the IFCs, successful calculations of lattice thermal conductivity have been reported for silicon [5, 6, 72], diamond [73], half-Heusler compounds [7], lead chalcogenides [74, 75], and gallium arsenide [76]. Such force field can be certainly used in NEMD, which is discussed in the following.

The anharmonic IFCs can be expressed in the form of Taylor expansion around the equilibrium atomic positions,

$$F_{i,\alpha} = -\Pi_{i,\alpha} - \sum_{j,\beta} \Phi_{i,j}^{\alpha,\beta} u_{j,\beta} - \frac{1}{2!} \sum_{jk,\beta\gamma} \Psi_{ijk}^{\alpha\beta\gamma} u_{j,\beta} u_{k,\gamma} - \frac{1}{3!} \sum_{jkl,\beta\gamma\delta} \mathrm{X}_{ijkl}^{\alpha\beta\gamma\delta} u_{j,\beta} u_{k,\gamma} u_{l,\delta} \,, \quad (6)$$

where, Φ, Ψ, and X are the harmonic, cubic, and quartic IFCs. The indices i, j, k, and l are the atom indices, and α, β, γ, and δ represent the Cartesian components. One way to calculate the anharmonic IFCs is the real space displacement method [77]. In this method, sets of force-displacement data are calculated while displacing the atoms from the equilibrium positions. The Hellman-Feynman forces can be obtained by DFT calculations in conventional supercell (typically about 100 atoms). Equation (6) is then fitted to the obtained force-displacement data, taking the translational and rotational invariance conditions into account.

The anharmonic IFCs are usually used for lattice dynamics calculations since they are convenient to calculate phonon properties (heat capacity, group velocity, relaxation time) through dynamical matrix and Fermi's golden rules. Application of the force field to MD simulation is somewhat tricky since the even order terms in the expansion makes the system unstable to large displacements under realistic temperatures. However, this can be remedied to some extent by collecting the force-displacement data giving weight to realize stable simulation [78]. Figure 6 shows the result of direct NEMD simulation of PbTe crystals. The calculations were performed for various lengths, and the bulk

thermal conductivity was calculated using the extrapolation method in Eq. (4). The obtained bulk lattice thermal conductivity was 2.1 $Wm^{-1}K^{-1}$ at 300 K [79], which is in good agreement with the experimental value 2.2 $Wm^{-1}K^{-1}$ [80, 81]. Note that MD, being a real space method, has an advantage over the lattice dynamics in the simplicity to treat local structures such as impurities and defects [78].

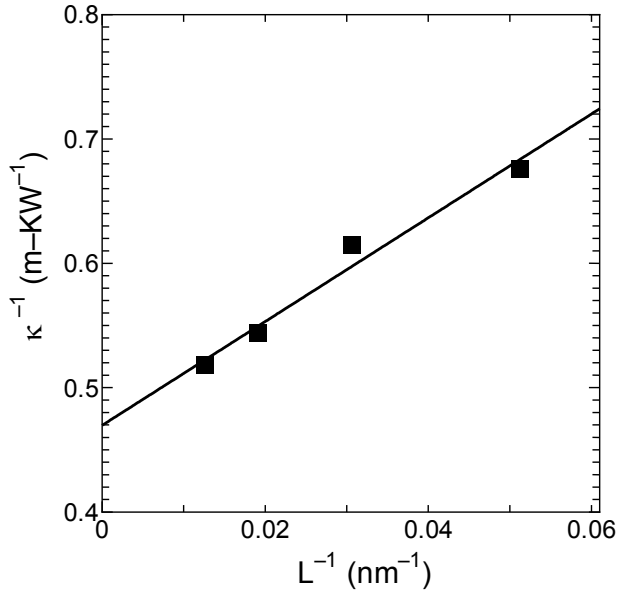

Fig. 6 Extraction of the bulk thermal conductivity of PbTe. The size dependent values were calculated using the direct NEMD method based on the interatomic force constants obtained from first principles [79].

2.2 Homogeneous method

As mentioned above, the direct NEMD method has advantage over the GK method by realizing faster convergence. On the other hand, the direct method usually requires large temperature gradient and heat flux, often resulting in nonlinear temperature profiles near the heat sink and source. The homogeneous NEMD (HNEMD) method [18, 82-84] lies in between the GK and the direct method. It also aims to achieve fast convergence by perturbing the system with the fictitious force, but keeps the perturbation small so that resulting nonequilibrium system can be described with equilibrium time correlation functions. This is done by extending the linear response theory to non-equilibrium distribution functions [18].

In the framework of linear response theory the equation of motion of the monoatomic system is written as

$$\begin{aligned}\dot{\mathbf{r}}_i &= \frac{\mathbf{p}_i}{m} + \mathbf{F}_e(t)\mathbf{C}_i(\mathbf{r}_i,\mathbf{p}_i) \\ \dot{\mathbf{p}}_i &= \mathbf{F}_i + \mathbf{F}_e(t)\mathbf{D}_i(\mathbf{r}_i,\mathbf{p}_i)\end{aligned}, \tag{7}$$

where ($\mathbf{r}_i$, $\mathbf{p}_i$) is the phase space information of *i*th atom. Here the canonical system with Hamiltonian H_0 ($\dot{\mathbf{r}}_i = \partial H_0/\partial \mathbf{p}_i$, $\dot{\mathbf{p}}_i = -\partial H_0/\partial \mathbf{r}_i$) is coupled with an external time dependent perturbation $\mathbf{F}_e$(t) through the phase variables $\mathbf{C}_i$ and $\mathbf{D}_i$. The rate of changes of the internal energy due to the external force is expressed as

$$\dot{H}_0(\mathbf{r}_i,\mathbf{p}_i,t) = \mathbf{A}(\mathbf{r}_i,\mathbf{p}_i)\mathbf{F}_e(t) \tag{8}$$

Due to the perturbation by the external force $\mathbf{F}_e(t)$, the distribution function changes from the canonical distribution function to non-canonical distribution function $f(\mathbf{r}_i, \mathbf{p}_i, t)$.

We now write down the ensemble average of an arbitral phase variable $\mathbf{B}(\mathbf{r}_i, \mathbf{p}_i, t)$ as

$$\left\langle \widetilde{\mathbf{B}}(t) \right\rangle = \int_{\Omega} \mathbf{B}(\mathbf{r}_i,\mathbf{p}_i) f(\mathbf{r}_i,\mathbf{p}_i,t) \mathrm{d}\mathbf{r}_i \mathrm{d}\mathbf{p}_i \tag{9}$$

By using linearized Liouville equation, which gives the non-canonical distribution as a function of $\mathbf{F}_e$ and $\mathbf{A}$, assuming $\mathbf{F}_e$ to be time independent, at a steady nonequilibrium state, we obtain,

$$\left\langle \widetilde{\mathbf{B}}(t) \right\rangle = \left\langle \widetilde{\mathbf{B}}(t) \right\rangle + \frac{\mathbf{F}_e}{k_B T} \int_0^t \left\langle \widetilde{\mathbf{B}}(t-t')\widetilde{\mathbf{A}}(0) \right\rangle_c \mathrm{d}t' , \tag{10}$$

where subscript *c* denotes the canonical ensemble. Now by choosing the heat flux vector $\mathbf{q}(\mathbf{r}_i, \mathbf{p}_i)$ to be the phase variable $\mathbf{B}(\mathbf{r}_i, \mathbf{p}_i)$ satisfying $\left\langle \mathbf{q}(\mathbf{r}_i,\mathbf{p}_i) \right\rangle_c = 0$, and with the GK formula for thermal conductivity reading,

$$\kappa = \frac{V}{k_B T^2} \int_0^t \left\langle q(t') \cdot q(0) \right\rangle_c \mathrm{d}t' , \tag{11}$$

we obtain,

$$\kappa = \lim_{t\to\infty} \lim_{F_e,\varepsilon \to \infty} \frac{\langle q(t) \rangle}{VTF_e} , \tag{12}$$

where q and F_e are the components of $\widetilde{\mathbf{q}}$ and $\mathbf{F}_e$ in the direction of heat conduction.

The appropriate phase variables in Eq. (7) for pair potential has been derived as

followings,

$$\mathbf{F}_e \mathbf{C}_i = 0$$

$$\mathbf{F}_e \mathbf{D}_i = (E_i - \overline{E})\mathbf{F}_e + \frac{1}{2}\sum_j \mathbf{F}_{ij}(\mathbf{r}_{ij} \cdot \mathbf{F}_e) - \frac{1}{2N}\sum_{j,k} \mathbf{F}_{jk}(\mathbf{r}_{jk} \cdot \mathbf{F}_e). \quad (13)$$

The algorithm has been extended to many-body potentials [85, 86] and mixed species systems [87, 88].

In order to calculate bulk thermal conductivity, the method requires multiple simulations for different values of F_e and extrapolation to $F_e \rightarrow 0$. There is certain ambiguity to the range of F_e. Too small F_e would make the external force field ineffective compared to the background thermal noise, and too large F_e would result in strongly nonequilibrium states with nonlinear dependence [86]. Appropriate range of F_e has been discussed in terms of kinetic theory for phonon gas [86] although the analysis so far is still limited to single scale (gray) phonon transport. Note that, for a quasi-ballistic system, similarly to the GK method, the method also requires the validation of the size effect to account for the missing contribution from the long wavelength phonons. Further development of these analyses may make the HNEMD method more accessible to wider researchers. Nevertheless, it has been shown that calculated thermal conductivity agrees with other methods [18, 86] and this has encouraged applications of the method to various systems including nanotubes [89-91] and nanowires [92].

2.3 Transient method

Transient NEMD method provides intuitive picture of heat propagation. The basic idea is to transiently apply local temperature perturbation and directly observe the diffusion of heat [Fig. 1(c)]. A few have applied such method to calculate thermal conductivity from the transient behavior. For instance, Daly *et. al.* [93] has performed a transient simulations of GaAs/AlAs supperlattice with sinusoidal temperature perturbation and the extracted thermal conductivity was later shown to agree with the direct method [50]. Applicability of the transient method to extract thermal conductivity from ab-initio molecular dynamics has also been demonstrated [94].

On the other hand, more common use of the transient NEMD is to investigate transient thermal phenomena, such as propagation of local heat. This is motivated by the investigation of the non-Fourier heat conduction or heat wave, which has long history and vast early literature some in relation with the second sound [95]. The deviation of nonstationary heat conduction from the fully diffusive Fourier's law description has

been known to become significant when the time and length scales of the system are within certain temporal and spatial windows of relaxation. Such non-Fourier heat conduction characteristics has been discussed by models based on microscopic phonon transport and the macroscopic continuum approaches, which reach similar expressions that suggest the collective phonons or heat propagating in a wavelike form at a certain speed [96, 97]. While models are limited to systems with weak nonlinearity, Tsai and MacDonald [98] were the first to perform NEMD simulations to examine the propagation of a heat wave under strongly anharmonic conditions. Later, Volz et al. [99] carried out NEMD simulations of thermally perturbed solid argon and compared the results with the Cattaneo-Vernotte equation [96, 97]. This has been recently explored with materials with long phonon mean free paths such as nanotubes and nanowires [100-103].

Further attempts have been carried out to apply various macroscopic non-Fourier heat conduction equations to the spatiotemporal temperature profiles obtained by transient NEMD. The work on CNT [100] shows that the conventional hyperbolic diffusion equation [96, 97] fails to predict the heat conduction due to the lack of local diffusion but this can be remedied by adopting a model with dual relaxation time [104, 105]. The transient NEMD can also be used to probe events with different time scales. The excitation and the evolution can be decomposed to temporal evolution of spectral bands, which reveals the quasi-ballistic features of the phonon transport [100-103]. This has been exercised to identify significant contribution of the optical phonons to CNT heat conduction [100].

3. THERMAL BOUNDARY CONDUCTANCE

Over the last decade, there has been an increasing interest to understand heat conduction across the interface since it dominates the overall heat conduction at the nanoscale. The NEMD method has been widely used to investigate the thermal boundary conductance at interfaces, reciprocal of the thermal boundary resistance (or Kapitza resistance [106, 107]). While alternatives would be the lattice dynamics method [108-110] or nonequilibrium Green's function methods [111], which give easier access to phonon transmission function and quantum effects, NEMD has advantages in its ability to handle complex structures and geometries, and including anharmonic effects without any assumptions (Recent developments in EMD techniques to obtain interfacial phonon transport is reviewed by Chalopin et. al. [112]). NEMD simulations are usually performed in inhomogeneous manners, either by steady method or transient method. The steady method can calculate intrinsic and interfacial thermal conductance at the

same time and is most commonly used. On the other hand, the transient method can be useful to identify multiple timescales imbedded in the phenomenon.

3.1 Steady state (direct) NEMD method

Considering two leads and an interface in the middle, one can calculate the thermal boundary conductance or resistance by modeling it as a serial connection of thermal resistances [113]. As illustrated in Fig. 7 (a, b), a typical approach is to first fit linear lines to the temperature profiles of the leads and extrapolate them to the location of the interface. Then by measuring the temperature jump at the interface location ΔT_j, the thermal boundary conductance is calculated as

$$G = q / \Delta T_j . \tag{14}$$

The method has been mostly applied to planer interfaces [114-118] but has also been applied to cylindrical configurations [119, 120] as shown in Fig. 7(c), which can be useful to compute interfacial thermal conductance in some nanocomposites. Here extrapolation is done based on the solution of the 1D-axisymmetric heat conduction equation ($C_1 \ln(r)+C_2$). Shenogin *et. al.* [120] calculated the thermal boundary conductance between a CNT and the octane matrix and obtained reasonable value in comparison with the experiments [121]. The steady method has been also applied to other classes of interface, such as in CNTs [122] and graphenes [123].

Numerous case studies have been carried out to gain insights into the mechanism of thermal boundary conductance using NEMD including effects of bulk modulus [124], temperature [114, 118, 124], interface bonding strength [124], and pressure [125]. These effects have been often discussed in terms of the vibrational mismatch models. For instance, it was shown for a silicon-amorphous polyethylene interface that the thermal boundary conductance decreases with stiffening the silicon. This was attributed to the enhancement of the effective mismatch, reduces the elastic phonon transport across the interface. On the other hand, it was shown that the thermal boundary conductance increases with temperature, suggesting the contribution of inelastic phonon transport.

Coming back to the methodology, one realizes that there is certain arbitrariness in the choice of the interface location. As in Fig. 7(a), if the interface is thermally sharp (atomically flat interface and localized or negligible strain/stress fields resulting in sharp temperature discontinuity), the interface can be located intuitively between the two materials. However, if each species diffuses into each other or the strain/stress field extends for a certain distance, the interface will have finite width. In such a case, one typically recognizes nonlinear temperature gradient in the interface region as illustrated

in Fig. 7(b) and the calculated thermal boundary conductance may depend on how the interface width and position are defined. A reasonable way is to define the entire region with nonlinear temperature as the interface region, and to extrapolate the linear temperature profiles to the midpoint of the interface region. This discussion becomes particularly relevant when taking into account the mass diffusion layer at the interface, which is expected to form at strong interfaces during the binding or deposition process. The NEMD simulations have shown that the presence of such layer with mix species can enhance thermal boundary conductance [126, 127], which opens up a possibility to engineer the interface to control heat flow.

Similarly to the previously discussed thermal conductivity calculations, the effect of simulation parameters on the obtained values needs to be examined. For instance, the leads and the thermostated part need to be long enough to account for the contribution from the long wave phonons, which usually have large interface transmittance, and to avoid the excess nonequilbrium phonon distribution caused by ballistic phonon transport. Since more length scales are involved than in the thermal conductivity calculations discussed in the previous section, the appropriate scaling of the size effects are not known. Nevertheless, a typical practice is to confirm the independence of the resulting thermal boundary conductance (or resistance) on the simulation parameters. Table 1 shows an example from Landry and McGaughey [118] on the interface between silicon and germanium crystals, where the effects of heat flux (q), lead length (L), thermostat length (L_c), cross sectional area (S), and orientation were checked.

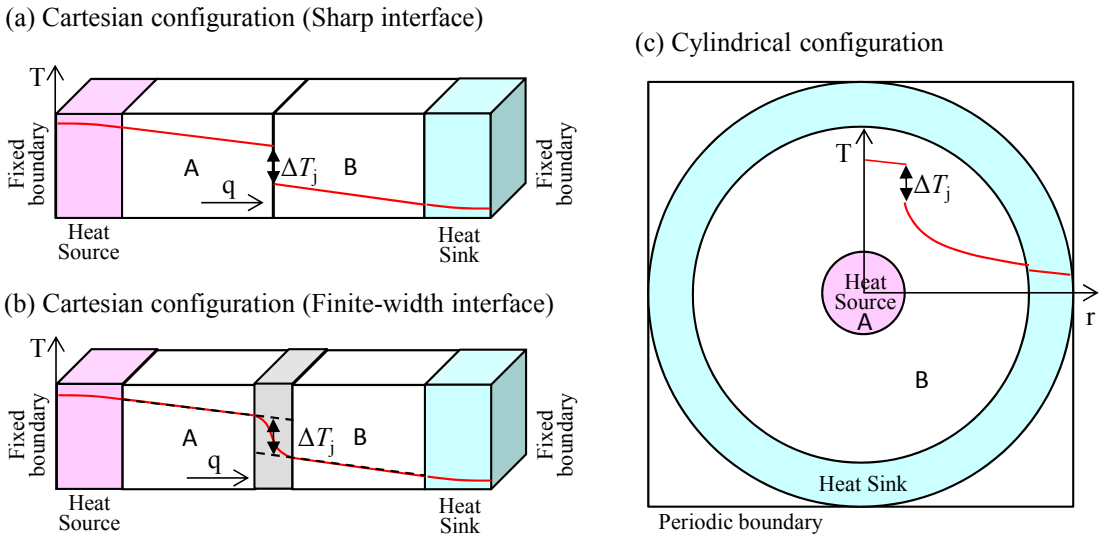

Fig. 7 Schematics of thermal boundary conductance calculations.

Table 1 Effect of direct NEMD simulation parameters on the thermal boundary resistance of the Si/Ge interface at 500 K [118]. *S* and *a* are the cross sectional area and the lattice constant parallel to the interface.

q (GWm^{-2})	L (monolayers)	L_c (monolayers)	S/a^2	Orientation	TBR, G^{-1} (10^{-9} m^2KW^{-1})
7.23	400	50	16	Si/Ge	2.93
7.23	400	50	16	Ge/Si	2.94
3.10	400	50	16	Si/Ge	3.02
13.4	400	50	16	Si/Ge	2.97
7.23	200	50	16	Si/Ge	4.01
7.23	300	50	16	Si/Ge	3.22
7.23	500	50	16	Si/Ge	2.72
7.23	600	50	16	Si/Ge	2.83
7.23	400	20	16	Si/Ge	3.17
7.23	400	100	16	Si/Ge	2.95
7.23	400	50	25	Si/Ge	3.13
7.23	400	50	36	Si/Ge	2.81

3.2 Transient method

When the thermal boundary resistance is much larger than the intrinsic thermal resistance of the two materials, the lumped heat capacity method can be applied. At this limit, the heat conduction between material A and material B can be considered as heat conduction between two thermal points with certain heat capacities. When A is instantaneously heated by ΔT_0 and then relaxed, the time history of the temperature difference between A and B follows $\Delta T=\Delta T_0\exp(-t/\tau_T)$ and gives the relaxation time τ_T of the interfacial heat conduction, which can be translated to thermal boundary conductance as follows.

$$G=\frac{1}{\left(\frac{1}{C_A}+\frac{1}{C_B}\right)S\tau_T}. \tag{15}$$

where *C* and S are the heat capacity and interfacial contact area, respectively.

Let us now compare the steady method and transient method. Such a comparison was first successfully carried out by Shenogin [120]. Here, a typical results of the steady

[Figure 8 (a)] and transient [Figure 8 (b)] methods are shown by taking the case of A:CNT and B:polyethylene (PE) interface in cylindrical configuration [Fig. 7(c)]. Figure 8(a) shows the temperature and density profiles of PE as functions of the distance from the CNT on applying steady heat flux. Figure 8(b) shows the relaxation of the temperature difference between the CNT and PE upon initially raising the CNT temperature by 100 K (ΔT_0=100 K). The thermal boundary conductance calculated by the two methods were 16.6 $MWm^{-2}K^{-1}$ and 15.3 $MWm^{-2}K^{-1}$ at 500 K, respectively, confirming the validity of the methods for the CNT-PE system.

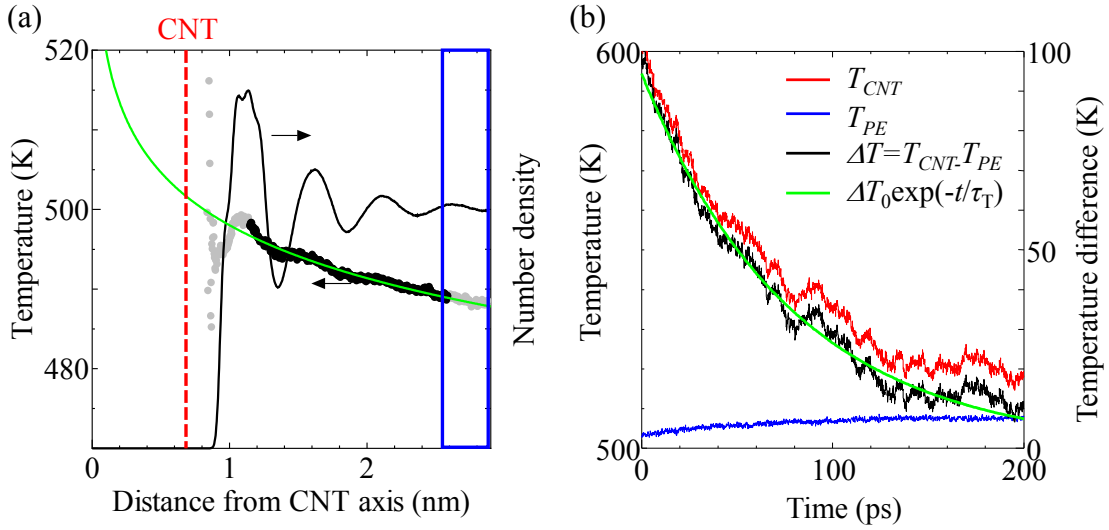

Fig. 8 (a) The steady NEMD simulations of a CNT-polyethylene system. The average temperature and number density profiles of polyethylene. The solid line denotes the fitting curve of the temperature profile. (b) The transient NEMD simulations. Averaged time histories of CNT temperature, PE temperature, and their difference. The temperature difference is fitted with an exponential function [128].

Similarly to the thermal conductivity calculation, the transient method can be also useful to identify multiple timescales in heat conduction across the interface. The simplest case is the dependence of thermal boundary conductance on the phonon frequencies. This can be done by calculating the phonon energy spectrum within a short time window Δt and observing the relaxation of the frequency dependent thermal energy. The phonon energy spectrum can be extracted by calculating the power spectral density of the velocity fluctuations [100],

$$g(f,t)=\frac{1}{N\Delta t}\sum_{j}^{N}\left|\int_{t-\Delta t/2}^{t+\Delta t/2}\mathbf{v}_j(t')e^{-2\pi ift'}\mathrm{d}t'\right|^2, \tag{16}$$

where f is the frequency, v_j is the velocity vector of jth atom, and N is the number of atoms in the heated material (A).

When A is momentarily heated with the equilibrium phonon distribution, the mode-dependent phonon transmission across the interface makes the distribution nonequilibrium, whose extent depends on the mode-dependent intrinsic and interfacial phonon scatterings and transmission. The frequency dependent thermal energy during the nonequilibrium process can be effectively quantified by introducing the spectral temperature,

$$T_{\mathrm{sp}}(f,t)=\frac{g(f,t)}{g^{\mathrm{eq}}(f)}T_{\mathrm{A}}, \tag{17}$$

where g^{eq} is the equilibrium spectrum of A at temperature T_{A}. For simplicity, if we assume the material B to be always in equilibrium at T_{B}, the relaxation of the spectral temperature can be written as,

$$\Delta T_{sp}(f,t)=T_{sp}(f,t)-T_B(t)=\Delta T_0\exp\left[-\frac{t}{\tau_T(f)}\right]. \tag{18}$$

The approach has been applied to CNT embedded in argon [129]. Since the full frequency analysis would require too many ensembles, the approach has been demonstrated by splitting the frequency range into the two regimes (1) low frequency regime, where the spectra of CNT and argon overlaps, and (2) high frequency regime, where they do not overlap. As shown in Fig. 9, the thermal energy in (1) relaxes to the argon matrix temperature much faster than that in (2). This demonstrates the dominant thermal boundary conductance in the frequency regime with spectral overlap between A and B, i.e. dominant role of elastic scattering.

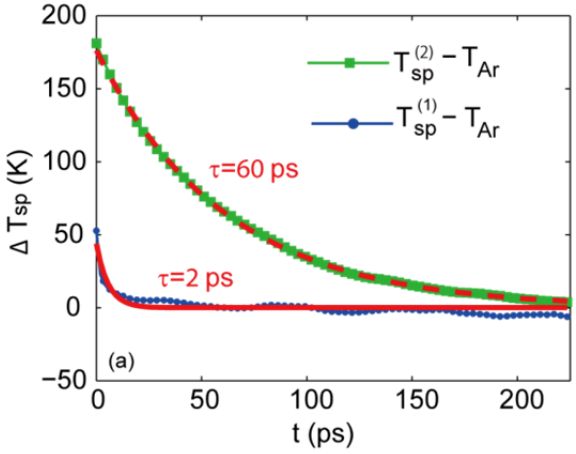

Fig. 9 Spectral temperature of instantaneously heated CNT in solid argon matrix. $T_{sp}^{(1)}$ and $T_{sp}^{(2)}$ are those of the low-frequency region and in the high-frequency region. The data denote the difference between $T_{sp}^{(1)}$ and T_{Ar} (green squares) and the difference between $T_{sp}^{(2)}$ and T_{Ar} (blue dots) fitting with single exponential functions.

4. SUMMARY

NEMD method with perturbation to the system involves several methodological issues, but when these are properly installed it could serve as a powerful tool to calculate thermal conductivity and thermal boundary conductance. Although the classical merit of realizing faster conversion than GK may have become less attractive with the growing accessibility to large ensembles with many-core clusters, the advantage of NEMD in the capability to handle complex structures and nanoscale properties have grown with nanotechnology. For instance, the most commonly used inhomogeneous steady methods enables us to calculate the classical size effect in thin films, nanotubes, graphene, and nanowires. Furthermore, for nanomaterials smaller than the simulation cell, NEMD can be applied to arbitral structures ranging from molecular chains to graded materials. Combined with ability to compute directional dependence, the method has been widely used to propose structures for thermal rectifier [130-133]. The steady and transient NEMD methods can probe local events in space and time. Thermal boundary conductance is a representative property, which can dominate heat conduction at small scale. With this capability and growing accessibility attributed to the various software packages, and with further improving the accuracy of the MD force fields, such as the interatomic force constants obtained from first principles, the NEMD methods are expected to become more useful to understand and design materials in various applications including thermal interface materials, nanostructured thermoelectrics, thermal insulating ceramics, phase change materials, and high power

transistors.

ACKNOWLEDGMENTS

The author would like to thank Shigeo Maruyama, Takahiro Yamamoto, Fredrik Carlborg, Sho Hida, Takuma Shiga, Takuma Hori, Takuru Murakami, Fuyuki Sugiura. This material is partially based upon work supported supported by Grant-in-Aid for Scientific Research (22226006 and 23760178) and Japan Science and Technology Agency, PRESTO.

REFERENCES

[1] J.E. Lennard-Jones, On the Determination of Molecular Fields, Proc. R. Soc. Lond. A, 106 (1924) 463.

[2] P.M. Morse, Diatomic Molecules according to the wave mechanics II. Vibrational levels, Phys. Rev., 34 (1929) 57.

[3] S. Maruyama, Molecular dynamics method for microscale heat transfer, Adv. Numer. Heat Transfer, 2 (2000) 189.

[4] A.J.H. McGaughey, M. Kaviany, Phonon Transport in Molecular Dynamics Simulations: Formulation and Thermal Conductivity, Advances in Heat Transfer, 39 (2006) 169.

[5] D.A. Broido, M. Malorny, G. Birner, N. Mingo, D.A. Stewart, Intrinsic lattice thermal conductivity of semiconductors from first principles, Appl. Phys. Lett., 91 (2007) 231922.

[6] K. Esfarjani, G. Chen, H.T. Stokes, Heat transport in silicon from first-principles calculations, Phys. Rev. B, 84 (2011) 085204.

[7] J. Shiomi, K. Esfarjani, G. Chen, Thermal conductivity of half-Heusler compounds from first-principles calculations, Phys. Rev. B, 84 (2011) 104302.

[8] G. Chen, Nanoscale Energy Transport and Conversion, Oxford University Press, New York, 2005.

[9] S. Plimpton, Fast parallel algorithms for short-range molecular dynamics, J. Comp. Phys., 117(1) (1995) 1.

[10] D.v.d. Spoel, E. Lindahl, B. Hess, G. Groenhof, A.E. Mark, H.J.C. Berendsen, GROMACS: Fast, flexible and free, J. Comp. Chem, 26 (2005) 1701.

[11] J.C. Phillips, R. Braun, W. Wang, J. Gumbart, E. Tajkhorshid, E. Villa, C. Chipot, D. Skeel, L. Kale, K. Schulten, Scalable molecular dynamics with NAMD, J. Comp. Chem, 26(1781) (2005).

[12] I.T. Todorov, W. Smith, K. Trachenko, M.T. Dove, DL_POLY_3: new dimensions in molecular dynamics simulations via massive parallelism, Mat. Chem., 16 (2006) 1911.

[13] J.R. Lukes, D.Y. Li, X.-G. Liang, C.-L. Tien, Molecular dynamics study of solid thin-film

thermal conductivity, J. Heat Transfer, 122 (2000) 536.
[14] P.K. Schelling, S.R. Phillpot, P. Keblinski, Comparison of atomic-level simulation methods for computing thermal conductivity, Phys. Rev. B, 65 (2002) 144.
[15] P. Chantrenne, J.-L. Barrat, Finite size effects in determination of thermal conductivities: comparing molecular dynamics results with simple models, J. Heat Transfer, 126 (2004) 577.
[16] A. Tenenbaum, G. Ciccotti, R. Gallico, Stationary nonequilibrium states by molecular dynamics Fourier's law, Phys. Rev. A 25 (1982) 2778.
[17] W.G. Hoover, W.T. Ashurst, Theor. Chem. Adv. Perspectives, 1 (1975) 2.
[18] D.J. Evans, Homogeneous NEMD algorithm for thermal conductivity: application of non-canonical linear response theory, Phys. Lett., 91A (1982) 457.
[19] D.H. Tsai, R.A. MacDonald, Phys. Rev. B, 14 (1976) 4714.
[20] S. Kotake, S. Wakuri, Molecular dynamics study of heat conduction in solid materials, JSME Int. J. B, (37) (1994).
[21] R.D. Mountain, R.A. MacDonald, Thermal conductivity of crystals: a molecular dynamics study of heat flow in a two-dimensional crystal, Phys. Rev. B, 28 (1983) 3022.
[22] S. Maruyama, A molecular dynamics simulation of heat conduction of a finite length single walled nanotube, Microscale Therm. Eng., 7 (2003) 41.
[23] J. Shiomi, S. Maruyama, Diffusive-Ballistic Heat Conduction of Carbon Nanotubes and Nanographene Ribbons, Int. J. Thermophys., 31:1945 (2007) 1945.
[24] A. Cao, J. Qu, Size dependent thermal conductivity of single-walled carbon nanotubes, J. Appl. Phys., 112 (2012) 013503.
[25] J. Shiomi, S. Maruyama, Molecular Dynamics of Diffusive-Ballistic Heat Conduction in Single-Walled Carbon Nanotubes, Jpn. J. Appl. Phys., 47 (2008) 2005.
[26] B. Hafsljold, S.K. Ratkje, Criteria for Local Equilibrium in a System with Transport of Heat and Mass, J. Stat. Phys., 78 (1995) 463.
[27] S. Nose, A unified formulation of the constant temperature molecular dynamics methods, J. Chem. Phys., 81 (1984) 511.
[28] W.G. Hoover, Canonical dynamics: Equilibrium phase-space distributions, Phys. Rev. A, 31 (1985) 1695.
[29] S.A. Adelman, J.D. Doll, Generalized Langevin equation approach for atom/solid-surface scattering: General formulation for classical scattering off harmonic solids, J. Chem. Phys., 64 (1975) 2375.
[30] F. Muller-Plathe, A simple nonequilibrium molecular dynamics method for calculating the thermal conductivity, J. Chem. Phys. , 106 (1997) 6082.
[31] T. Ikeshoji, B. Hafsljold, Non-equilibrium molecular dynamics calculation of heat

conduction in liquid and through liquid-gas interface, Mol. Phys., 81 (1994) 251.
[32] R. Bedrov, G.D. Smith, Thermal conductivity of molecular fluids from molecular dynamics simulations: application of a new imposed-flux method, J. Chem. Phys. Lett., 113 (2000) 8080.
[33] P. Jund, R. Jullien, Molecular-dynamics calculation of the thermal conductivity of vitreous silica, Phys. Rev. B, 59 (1999) 13707.
[34] R.D. Mountain, System size and control parameter effects in reverse perturbation nonequilibrium molecular dynamics, J Chem Phys., 124 (2006) 104109.
[35] R. Peierls, Quantum Theory of Solids, Clarendon, Oxford, 1955.
[36] N. Mingo, D.A. Broido, Length Dependence of Carbon Nanotube Thermal Conductivity and the "Problem of Long Waves", Nano Lett., 5 (2005) 1221.
[37] Z. Tian, K. Esfarjani, J. Shiomi, A.S. Henry, G. Chen, On the importance of optical phonons to thermal conductivity in nanostructures, Appl. Phys. Lett., 99 (2011) 053122.
[38] T. Yamamoto, S. Konabe, J. Shiomi, S. Maruyama, Crossover from Ballistic to Diffusive Thermal Transport in Carbon Nanotubes, Appl. Phys. Express, 2 (2009) 095003.
[39] L.G.C. Rego, G. Kirczenow, Quantized Thermal Conductance of Dielectric Quantum. Wires, Phys. Rev. Lett., 81 (1998) 232.
[40] T. Yamamoto, S. Watanabe, K. Watanabe, Universal Features of Quantized Thermal Conductance of Carbon Nanotubes, Phys. Rev. Lett., 92 (2004) 075502.
[41] H.B.G. Casimir, Physica (Amsterdam), 6 (1938) 495.
[42] P.G. Klemens, D.F. Pedraza, Theory of the a-Plane Thermal Conductivity of Graphite, Carbon, 32 (1994) 735.
[43] Y.-G. Yoon, R. Car, D.J. Srolovitz, S. Scandolo, Thermal conductivity of crystalline quartz from classical simulations, Phys. Rev. B, 70 (2004) 012302.
[44] P.K. Schelling, S.R. Phillpot, Mechanism of thermal transport in zirconia and yttria-stabilized zirconia by molecular-dynamics simulation., J. Am.Ceram. Soc., 84 (2001) 2997.
[45] K. Konashi, T. Ikeshoji, Y. Kawazoe, H. Matsui, A molecular dynamics study of thermal conductivity of zirconium hydride, J. Alloy. Compd, 356 (2003) 279.
[46] M.A. Osman, D. Srivastava, Temperature dependence ofthe thermal conductivity of single-wall carbon nanotubes, Nanotechnology, 12 (2001) 21.
[47] T. Luo, K. Esfarjani, J. Shiomi, A. Henry, G. Chen, Molecular dynamics simulation of thermal energy transport in polydimethylsiloxane, J. Appl. Phys., 109 (2011) 074321.
[48] D.P. Sellan, E.S. Landry, J.E. Turney, A.J.H. McGaughey, C.H. Amon, Size effects in molecular dynamics thermal conductivity predictions, Phys. Rev. B, 81 (2010) 214305.
[49] X.-G. Liang, B. Shi, Two-dimensional molecular dynamics simulation of the thermal

conductance of superlattices, Mater Sci. Eng. A Struct., 292 (2000) 198.
[50] K. Imamura, Y. Tanaka, N. Nishiguchi, S. Tamura, Lattice thermal conductivity in superlattices: molecular dynamics calculations with a heat reservoir method, J. Phys.: Condens. Matter, 15(8679) (2003).
[51] Y. Chen, D. Li, J. Yang, Y. Wu, J.R. Lukes, A. Majumdar, Molecular dynamics study of the lattice thermal conductivity of Kr/Ar superlattice nanowires, Physica B, 349 (2004) 270.
[52] A.R. Abramson, C.-L. Tien, A. Majumdar, Interface and strain effects on the thermal conductivity of heterostructures: a molecular dynamics study, J. Heat Transfer, 124 (2002) 963.
[53] M. Hu, D. Poulikakos, Si/Ge Superlattice Nanowires with Ultralow Thermal Conductivity, Nano Lett., 12 (2012) 5487.
[54] J. Shiomi, S. Maruyama, Heat conduction of single-walled carbon nanotube isotope superlattice structures: A molecular dynamics study, Phys. Rev. B, 74 (2006) 155401
[55] E.G. Noya, D. Srivastava, L.A. Chernozatonskii, M. Menon, Thermal conductivity of carbon nanotube peapods, Phys. Rev. B, 70 (2004) 115416.
[56] R.H.H. Poetzsch, H. Bottger, Interplay of disorder and anharmonicity in heat conduction: molecular-dynamics study, Phys. Rev. B, 50 (1994) 15757.
[57] J.R. Lukes, C.-L. Tien, Molecular dynamics simulation of thermal conduction in nanoporous thin films, Microscale Therm. Eng., 8 (2004) 341.
[58] Y. He, I. Savic, D. Donadio, G. Galli, Lattice thermal conductivity of semiconducting bulk materials: atomistic simulations, Phys. Chem. Chem. Phys., 14 (2012) 16209.
[59] C. Oligschleger, J.C. Schon, Simulation of thermal conductivity and heat transport in solids, Phys. Rev. B, 59 (1999) 4125.
[60] J. Michalski, Thermal conductivity of amorphous solids above the plateau: molecular-dynamics study, Phys. Rev. B, 45 (1992) 7054.
[61] P. Heino, E. Ristolainen, Thermal conduction at the nanoscale in some metals by MD, Microelectr. J, 34 (2003) 773.
[62] J.E. Turney, E.S. Landry, A.J.H. Mcgaughey, C.H. Amon, Phys. Rev. B, 79 (2009) 064301.
[63] E.S. Landry, A.J.H. McGaughey, Effect of interfacial species mixing on phonon transport in semiconductor superlattices, Phys. Rev. B, 79 (2009) 075316.
[64] B. Ni, T. Watanabe, S.R. Phillpot., Thermal transport in polyethylene and at polyethylene-diamond interfaces investigated using molecular dynamics simulation, J. Phys.: Condens. Matter, 21 (2009) 084219.
[65] L. Shi, D. Yao, G. Zhang, B. Li, Size dependent thermoelectric properties of silicon nanowires, Appl. Phys. Lett., 95 (2009) 063102.

[66] S.-C. Wang, X.-G. Liang, X.-H. Xu, T. Ohara, Thermal Conductivity of Silicon Nanowire by Nonequilibrium Molecular Dynamics Simulations, J. Appl. Phys., 105 (2009) 014316.
[67] N. Papanikolaou, Lattice thermal conductivity of SiC nanowires J. Phys.: Condens. Matter, 20 (2008) 135201.
[68] A. Ward, D.A. Broido, Intrinsic phonon relaxation times from first-principles studies of the thermal conductivities, Phys. Rev. B, 81 (2010) 085205.
[69] F.H. Stillinger, T.A. Weber, Computer simulation of local order in condensed phases of silicon, Phys. Rev. B, 31 (1985) 5262.
[70] J. Tersoff, Empirical interatomic potential for silicon with improved elastic properties, Phys. Rev. B, 38 (1988) 9902.
[71] D.A. Broido, A. Ward, N. Mingo, Lattice thermal conductivity of silicon from empirical interatomic potentials, Phys. Rev. B, 72 (2005) 014308.
[72] J. Garg, N. Bonini, B. Kozinsky, N. Marzari, Role of Disorder and Anharmonicity in the Thermal Conductivity of Silicon-Germanium Alloys:
A First-Principles Study, Phys. Rev. Lett., 106 (2011) 045901.
[73] A. Ward, D.A. Broido, D.A. Stewart, G. Deinzer, Ab initio theory of the lattice thermal conductivity in diamond, Phys. Rev. B, 80 (2009) 125203.
[74] T. Shiga, J. Shiomi, J. Ma, O. Delaire, T. Radzynski, A. Lusakowski, K. Esfarjani, G. Chen, Microscopic mechanism of low thermal conductivity in lead telluride, Phys. Rev. B, 72(014308) (2005).
[75] Z. Tian, J. Garg, K. Esfarjani, T. Shiga, J. Shiomi, G. Chen, Phonon conduction in PbSe, PbTe, and PbTe1−xSex from first-principles calculations, Phys. Rev. B, 85 (2012) 184303.
[76] T. Luo, J. Garg, J. Shiomi, K. Esfarjani, G. Chen, Gallium arsenide thermal conductivity and optical phonon relaxation times from first-principles calculations, EPL, 101 (2013) 16001.
[77] K. Esfarjani, H.T. Stokes, Method to extract anharmonic force constants from first principles calculations, Phys. Rev. B, 77 (2008) 144112.
[78] T. Murakami, T. Shiga, T. Hori, K. Esfarjani, J. Shiomi, Importance of local force fields on lattice thermal conductivity reduction in PbTe1−xSex alloys, Europhys. Lett., 102 (2013) 46002.
[79] F. Sugiura, T. Murakami, T. Hori, T. Shiga, J. Shiomi, unpublished.
[80] I.U.I. Ravich, B.A. Efimova, I.A. Smirnov, Semiconducting Lead Chalcogenides, Plenum Press, New York, 1970.
[81] V.I. Fedorov, V.I. Machuev, Sov. Phys. Solid State USSR, 11 (1969) 1116.
[82] M.J. Gillian, M. Dixon, The calculation of thermal conductivity by perturbed molecular simulation, J. Phys. C Solid state, 16 (1983) 869.

[83] P.J. Daivis, D.J. Evans, Non-equilibrium molecular dynamics calculation of thermal conductivity of flexible molecules: butane, Mol. Phys., 81 (1994) 1289.
[84] A. Perronace, J.-M. Simon, B. Rousseau, G. Ciccotti, An International Journal at the Interface Between Chemistry and Physics, Mol. Phys., 99 (2001) 1139.
[85] K.K. Mandadapu, R.E. Jones, P. Papadopoulos, Generalization of the homogeneous nonequilibrium molecular dynamics method for calculating thermal conductivity to multibody potentials, Phys. Rev. E, 80 (2009) 047702.
[86] K.K. Mandadapu, R.E. Jones, P. Papadopoulos, A homogeneous nonequilibrium molecular dynamics method for calculating thermal conductivity with a three-body potential, J. Chem. Phys., 130 (2009) 204106.
[87] D.J. Evans, P.T. Cummings, Non-equilibrium molecular dynamics algorithm for the calculation of thermal diffusion in simple fluid mixtures, Molecular Physics, 72 (1991) 893.
[88] K.K. Mandadapu, R.E. Jones, P. Papadopoulos, A homogeneous nonequilibrium molecular dynamics method for calculating the heat transport coefficient of mixtures and alloys, J. Chem. Phys., 133 (2010) 034122.
[89] S. Berber, Y.-K. Kwon, D. Tománek, Unusually High Thermal Conductivity of Carbon Nanotubes, Phys. Rev. Lett., 84 (2000) 4613.
[90] Z. Wang, F. Gao, J.-P. Crocombette, X.T. Zu, L. Yang, W.J. Weber, Thermal conductivity of GaN nanotubes simulated by nonequilibrium molecular dynamics, Phys. Rev. B, 75 (2007) 153303.
[91] J.R. Lukes, H. Zhong, Thermal Conductivity of Individual Single-Wall Carbon Nanotubes, J. Heat Transfer, 129 (2007) 705.
[92] Z. Wang, X. Zu, F. Gao, W.J. Weber, J.-P. Crocombette, Atomistic simulation of the size and orientation dependences of thermal conductivity in GaN nanowires, Appl. Phys. Lett., 90 (2007) 161923.
[93] B.C. Daly, H.J. Maris, K. Imamura, S. Tamura, Molecular dynamics calculation of the thermal conductivity of superlattices, Phys. Rev. B, 66 (2002) 024301.
[94] T.M. Gibbons, S.K. Estreicher, Impact of Impurities on the Thermal Conductivity of Semiconductor Nanostructures: First-Principles Theory, Phys. Rev. Lett., 102 (2009) 255502.
[95] D.D. Joseph, L. Preziosi, Heat waves, Rev. Mod. Phys., 62 (1990) 375.
[96] C. Cattaneo, A form of heat conduction equation which eliminates the paradox of instantaneous propagation, C. R. Hebd. Seances Acad. Sci., 247 (1958) 431.
[97] P. Vernotte, Les Paradoxes de la Theorie Continue de l'equation De La Chaleur, C. R. Hebd. Seances Acad. Sci., 246 (1958) 3154.
[98] D.H. Tsai, R.A. MacDonald, Molecular-dynamical study of second sound in a solid excited by a strong heat pulse, Phys. Rev. B, 14 (1976) 4714

[99] S. Volz, J.B. Saulnier, M. Lallemand, B. Perrin, P. Depondt, M. Mareschal, Transient Fourier-law deviation by molecular dynamics in solid argon, Phys. Rev. B, 54 (1996) 340.
[100] J. Shiomi, S. Maruyama, Non-Fourier heat conduction in a single-walled carbon nanotube: Classical molecular dynamics simulations, Phys. Rev. B, 73(20) (2006) 205420.
[101] M.A. Osman, D. Srivastava, Molecular dynamics simulation of heat pulse propagation in single-wall carbon nanotubes, Phys. Rev. B, 72 (2005) 125413.
[102] M. Wang, N. Yang, Z.-Y. Guo, Non-Fourier heat conductions in nanomaterials
J. Appl. Phys., 110 (2011) 064310.
[103] X. Zhang, M. Hu, D. Poulikakos, A Low-Frequency Wave Motion Mechanism Enables Efficient Energy
Transport in Carbon Nanotubes at High Heat Fluxes, Nano Lett., 12 (2012) 3410.
[104] D.Y. Tzou., A Unified Field Approach for Heat Conduction From Macro- to Micro-Scales, J. Heat Transfer, 117 (1995) 8.
[105] D.W. Tang, N. Araki, Wavy, wavelike, diffusive thermal responses of finite rigid slabs to high-speed heating of laser-pulses, Int. J. Heat Mass Transfer, 42 (1999) 855.
[106] P.L. Kapitza, The Study of Heat Transfer on Helium II, J. Phys. USSR, 4 (1941) 181.
[107] E.T. Swartz, R.O. Pohl, Thermal boundary resistance, Rev. Mod. Phys., 61(3) (1989) 605.
[108] D.A. Young, H.J. Maris, Lattice-dynamical calculation of the Kapitza resistance between fcc lattices, Phys. Rev. B, 40 (1989) 3685.
[109] H. Zhao, J.B. Freund, Lattice-dynamical calculation of phonon scattering at ideal Si–Ge interfaces J. Appl. Phys., 97(024903) (2005).
[110] J. Wang, J. Wang, Characteristics of phonon transmission across epitaxial interfaces: a lattice dynamic study J. Phys.: Condens. Matter, 19 (2007) 236211.
[111] W. Zhang, T.S. Fisher, N. Mingo, Simulation of Interfacial Phonon Transport in Si–Ge Heterostructures Using an Atomistic Green's Function Method, ASME J. Heat Transfer, 129 (2007) 483.
[112] Y. Chalopin, A. Rajabpour, H. Han, Y. Ni, S. Volz, Equilibrium Molecular Dynamics Simulations on Interfacial Phonon Transport, Annu. Rev. Heat Transfer, (2013).
[113] A. Maiti, G.D. Mahan, S.T. Pantelides, Dynamical simulations of nonequilibrium processes heat flow and the Kapitza resistance across grain boundaries, Solid State Commun., 102 (1997) 517.
[114] R.J. Stevens, L.V. Zhigilei, P. M. Norris, Molecular-Dynamics Study of Thermal Boundary Resistance: Evidence of Strong Inelastic Scattering Transport Channels, Int. J. Heat Mass Tranfer, 50 (2007) 3977.
[115] C. Kimmer, S. Aubry, A. Skye, P.K. Schelling, Scattering of phonons from a high-energy

grain boundary in silicon: Dependence on angle of incidence, Phys. Rev. B, 75 (2007) 144105.
[116] S. Aubry, C.J. Kimmer, A. Skye, P.K. Schelling, Comparison of theoretical and simulation-based predictions of grain-boundary Kapitza conductance in silicon, Phys. Rev. B, 78 (2008) 064112.
[117] C.J. Twu, J.R. Ho., Molecular-dynamics study of energy flow and the Kapitza conductance across an interface with imperfection formed by two dielectric thin films, Phys. Rev. B, 67 (2003) 205422.
[118] E.S. Landry, A.J.H. McGaughey, Thermal boundary resistance predictions from molecular dynamics simulations and theoretical calculations, Phys. Rev. B, 80 (2009) 165304.
[119] S. Shenogin, A. Bodapati, R.O. L. Xue, P. Keblinski, Effect of chemical functionalization on thermal transport of carbon nanotube composites, Appl. Phys. Lett., 85 (2004) 2229.
[120] S. Shenogin, L. Xue, R. Ozisik, P. Keblinski, D.G. Cahill, Role of thermal boundary resistance on the heat flow in carbon-nanotube composites, J. Appl. Phys. , 95 (2004) 8136.
[121] S.T. Huxtable, D.G. Cahill, S. Shenogin, L. Xue, R. Ozisik, P. Barone, M. Usrey, M.S. Strano, G. Siddons, M. Shim, P. Keblinski, Interfacial heat flow in carbon nanotube suspensions, Nat. Mater. , 2 (2003) 731.
[122] H. Zhong, J. Lukes, Interfacial Thermal Resistance Between Carbon Nanotubes: Molecular Dynamics Simulations and Analytical Thermal Modeling, Phys. Rev. B, 74 (2006) 125403.
[123] A. Bagri, S.-P. Kim, R.S. Ruoff, V.B. Shenoy, Thermal transport across Twin Grain Boundaries in Polycrystalline Graphene from Nonequilibrium Molecular Dynamics Simulations, Nano Lett., 11 (2011) 3917.
[124] M. Hu, P. Keblinski, P.K. Schelling, Kapitza conductance of silicon–amorphous polyethylene interfaces by molecular dynamics simulations, Phys. Rev. B, 79 (2009) 104305.
[125] T. Luo, J.R. Lloyd, Non-equilibrium molecular dynamics study of thermal energy transport in Au–SAM–Au junctions, Int. J. Heat Mass Trans. , 53 (2010) 1.
[126] M. Matsumoto, H. Wakabayashi, T. Makino, Thermal Resistance of Crystal Interface: Molecular Dynamics Simulation Heat Transfer—Asian Research, 34 (2005).
[127] T.S. English, J.C. Duda, J.L. Smoyer, D.A. Jordan, P.M. Norris, L.V. Zhigilei, Enhancing and tuning phonon transport at vibrationally mismatched solid-solid interfaces, Phys. Rev. B, 85 (2012) 035438.
[128] S. Hida, T. Shiga, T. Hori, J. Elliott, J. Shiomi, Thermal resistance and phonon scattering at interface between carbon nanotube and polyethylene, International Journal of Heat and Mass Transfer, (in press) (2013).

[129] C.F. Carlborg, J. Shiomi, S. Maruyama, Thermal boundary resistance between single-walled carbon nanotubes and surrounding matrices, Phys. Rev. B, 78 (2008) 205406.
[130] M. Alaghemandi, E. Algaer, M.C. Bohm, F. Muller-Plathe, The thermal conductivity and thermal rectification of carbon nanotubes studied using reverse non-equilibrium molecular dynamics simulations, Nanotechnology, 20 (2009) 115704.
[131] J. Hu, X. Ruan, Y.P. Chen, Thermal Conductivity and Thermal Rectification in Graphene Nanoribbons: A Molecular Dynamics Study, 9 (2009) 2730.
[132] G. Wu, B. Li, Thermal rectification in carbon nanotube intramolecular junctions: Molecular dynamics calculations, Phys. Rev. B, 76 (2007) 085424.
[133] N. Yang, G. Zhang, B. Li, Carbon nanocone: A promising thermal rectifier, Appl. Phys. Lett., 93 (2008) 243111.